Supersonic Noncircular Missile Computations

F. J. Priolo* and A. B. Wardlaw Jr.†
U.S. Naval Surface Warfare Center, Silver Spring, Maryland

The ZEUS program, which solves Euler's equations by spatial marching, is applied to missiles with noncircular cross sections. It incorporates a multiple-zone gridding technique and a second-order extension of Godunov's method. This Godunov method is an upwind scheme based on the Riemann problem for steady, supersonic flow and cast in a control volume formulation. Second-order accuracy is obtained by computing local slopes and adding a predictor step. The scheme fits the bow shock and captures imbedded shocks. Computational speeds can be improved by adopting an approximate Riemann solver. The program is applied to body-alone and body-wing-tail configurations with elliptic cross sections. Computed surface pressure distributions agree well with experiments on the windward and leeward surfaces with some discrepancies at the body shoulder. In this region, the inviscid results do not accurately model the crossflow separation and associated vortex development, but this discrepancy has little effect on the accurate prediction of the aerodynamic coefficients.

Nomenclature

A^n = area of control volume edge lying in the $z = z^n$ plane
$b(\phi,z)$ = radial position of edge 1 (Fig. 2)
C_M = pitching moment coefficient, pitching moment/$q_\infty SL$
C_N = normal force coefficient, normal force/$q_\infty S$
C_p = pressure coefficient, $(p - p_\infty)/q_\infty$
$c(\phi,z)$ = radial position of edge 3 (Fig. 2)
$\bar{F}$ = flux vector, Eq. (1)
H_0 = stagnation enthalpy
L = reference length, length of configuration
M_∞ = freestream Mach number
$\bar{n} = (n_x,n_y,n_z)$ = vector normal to cell edge, Eq. (1)
$|\bar{n}|$ = cell edge area
p = pressure
q_∞ = freestream dynamic pressure
$R_\pm$ = upper and lower supersonic streams for the Riemann problem (Fig. 4)
(r,ϕ,z) = cylindrical coordinates (Fig. 2)
S = reference area, maximum cross-sectional area of the body
$\bar{U}$ = flux vector, Eq. (1)
(u,v,w) = Cartesian velocity components
(x,y,z) = Cartesian coordinates with z along the missile axis
α = angle of attack
δ_f = flow direction angle (Fig. 4)
(ξ,η,ζ) = computational coordinates (Fig. 2)
γ = ratio of specific heats
κ' = difference limiter, Eq. (3)
ϕ = crossflow plane angle measured clockwise from the positive x axis
ρ = density
$\sigma(r,z)$ = angular location of edge 4 (Fig. 2)
$\psi(r,z)$ = angular location of edge 2 (Fig. 2)

Subscripts

i,j = cell center in the crossflow plane (Fig. 5)
∞ = ambient conditions

Introduction

TRADITIONALLY, missile aerodynamics has been predicted using semi-empirical methods that are based on an extensive data base. These methods determine the global aerodynamic characteristics using a minimum of computational resources. Numerical methods, on the other hand, are independent of experimental data but require a greater computational effort. Such techniques are applicable to a wider range of configurations and flight parameters and provide detailed flowfield properties not attainable using empirical methods. A number of numerical procedures have been applied to missiles. These include: linearized potential panel, nonlinear full potential, space marching Euler, time marching Euler, parabolized Navier-Stokes, thin-layer Navier-Stokes, and Reynolds-averaged Navier-Stokes. A survey of these methods is provided by Hoeijmakers.[1]

The present paper focuses on applying the Euler equations to missiles in supersonic flight. Under these conditions, the Euler equations are hyperbolic, and the missile's flowfield can be determined from known flow conditions at a cross-sectional plane near the nose tip. This initial data plane is marched down the length of the missile to the base as shown in Fig. 1. Computational times for a complete missile are similar to those for linear potential methods given by Ref. 1. However, the Euler equations can treat shocks of arbitrary

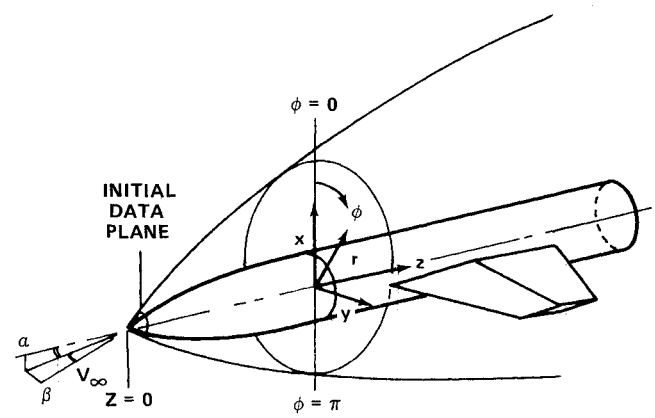

Fig. 1 Cartesian and cylindrical coordinate systems.

Presented as Paper 88-0278 at the AIAA 26th Aerospace Sciences Meeting, Reno, NV, Jan. 11-14, 1988; received April 25, 1988; revision received Nov. 23, 1988.

*Aerospace Engineer, Applied Mathematics Branch. Member AIAA.

†Aerospace Engineer, Applied Mathematics Branch. Associate Fellow AIAA.

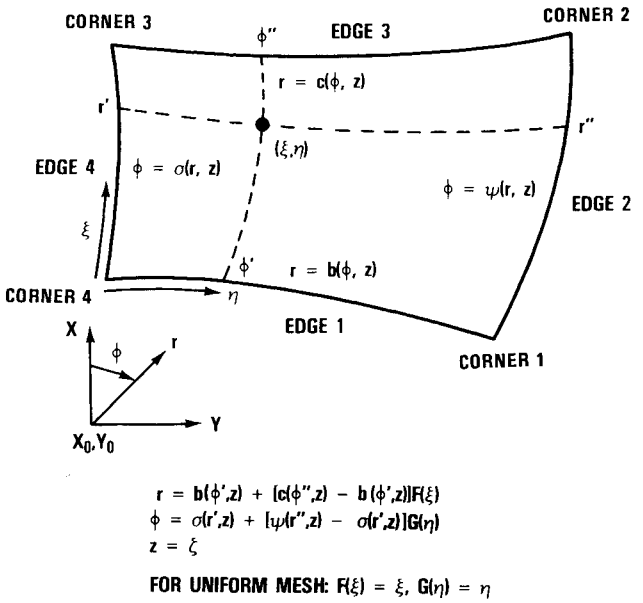

Fig. 2 Quadrilateral zone structure.

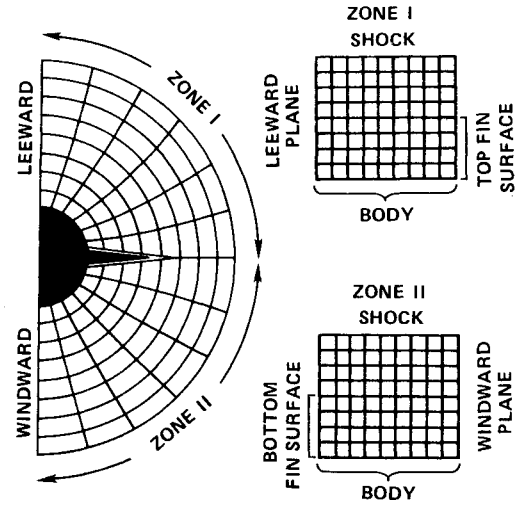

Fig. 3 Multiple-zone mesh.

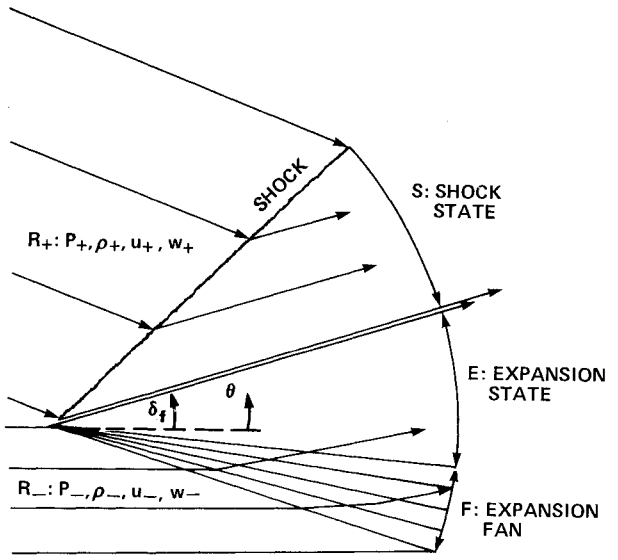

Fig. 4 The supersonic Riemann problem consists of two intersecting supersonic streams, R_+ and R_-.

strength and convect vorticity, whereas potential methods cannot. Vorticity generated by separation is not described by the Euler equations, and phenomena such as body vortices must be empirically modeled.

Space marching Euler methods were originally applied to re-entry vehicles that featured conical geometries complicated by cuts and flaps. Mesh generation was accomplished using a single transformation,[2-5] a technique that is not well suited to tactical missiles. Tactical missiles are characterized by thin, low-aspect-ratio fins with sharp edges, and solutions for these shapes have been accomplished using a multiple-zone strategy. Here a complicated flowfield is divided into several quadrilateral zones, each of which can be treated using a single mapping, as shown in Fig. 2. Zone boundaries are taken to coincide with the body, wing, and tracked bow shock surfaces. Initial work by Wardlaw et al.[6-10] applied the MacCormack scheme with characteristic boundary conditions. These characteristic boundary conditions are enforced at wing edges and surface discontinuities in conjunction with special procedures that apply oblique shocks and expansions where appropriate. These methods have been successfully applied to missiles but are not robust. For complex shapes, artificial viscosity and special procedures must be adjusted on a trial-and-error basis. Additionally, Wardlaw et al.[11] combined the same multiple-zone approach with Godunov's first-order method[12] for steady supersonic flow. Unlike the MacCormack approach, this technique is robust and devoid of any special procedures.

The zonal Euler solver (ZEUS) of Wardlaw et al.[13-15] is a space marching method that combines a simple, multiple-zone, gridding technique and a second-order extension of Godunov's method. The Godunov method is an upwind scheme based on the Riemann problem for steady supersonic flow. It is cast in control volume form and consists of a predictor and corrector step. The predictor step advances the primitive variables using Euler's equations in nonconservation form. Derivatives are computed using a limited central differencing procedure. The corrector step modifies Godunov's method by assuming linear property variations within each control volume. This program is devoid of explicit artificial viscosity and is robust.

The current paper applies the ZEUS program, first reported in Ref. 13, to several supersonic noncircular missile shapes and compares results to experiment. A brief description of the computational algorithm is provided with more details outlined in Refs. 13-15. The final two sections illustrate the results and draw some conclusions.

Computational Procedure

Code Structure

The ZEUS program uses a multiple-zone structure that provides a convenient framework from which to compute shapes having sharp-edged fins. The crossflow plane is divided into several quadrilateral zones, and a simple, separate transformation is applied to each. A general quadrilateral zone is displayed in Fig. 2 for cylindrical coordinates. The radial locations of edges 1 and 3 are described in terms of functions $b(\phi,z)$ and $c(\phi,z)$, while the angular positions of edges 2 and 4 are defined by $\psi(r,z)$ and $\sigma(r,z)$.

A typical multiple-zone structure for a missile, shown in Fig. 3, features the missile body and bow shock on opposite edges of quadrilateral zones. The fin surfaces are located on the remaining two edges of each zone. The number of grid points covered by the fin surfaces may change from one axial step to the next.

Numerical Scheme

For steady supersonic flow, the Riemann problem represents the confluence of two two-dimensional supersonic streams, as illustrated in Fig. 4. At the point of intersection, shocks or expansion fans form, which turn both streams to a common direction. The two final streams need not feature the same density or velocity and a slip line generally forms be-

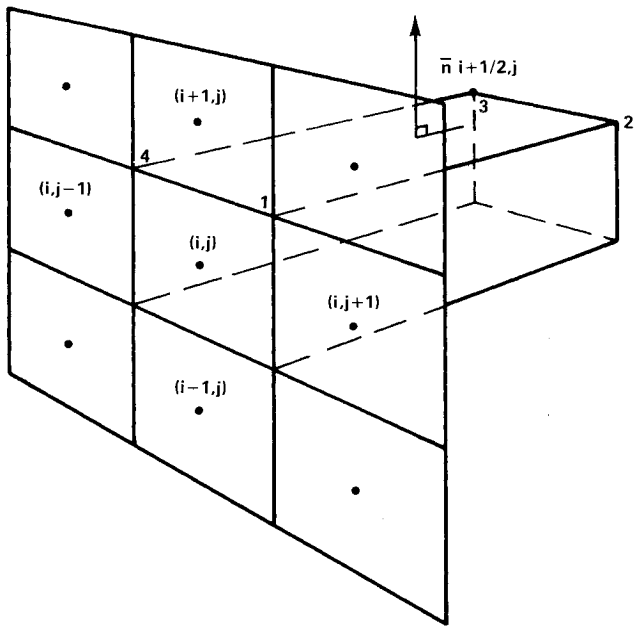

Fig. 5 Control volume nomenclature.

tween them. The solution begins by guessing the slip line orientation and computing the pressure on each side. Since the shock and expansion relations are nonlinear, an iterative procedure is adopted that adjusts the slip line orientation until the appropriate direction is found. This direction is the one producing the same pressure in both streams. If the two streams forming the Riemann problem have similar properties, a closed-form linear solution can be obtained. Alternatively, an approximate Riemann problem[16] can be constructed that has a closed-form solution.

Using the notation of Fig. 5, mass and momentum conservation through a control volume can be expressed as:

$$\bar{U}_{i,j}^{n+1} = \bar{U}_{i,j}^{n} - \bar{F}_{i+\frac{1}{2},j} + \bar{F}_{i-\frac{1}{2},j} - \bar{F}_{i,j+\frac{1}{2}} + \bar{F}_{i,j-\frac{1}{2}} \qquad (1a)$$

where

$$\bar{U}_{i,j}^{n} = A_{i,j}^{n} \begin{bmatrix} \rho w \\ \rho w^2 + p \\ \rho wu \\ \rho wv \end{bmatrix}_{i,j} \qquad \bar{F}_{i+\frac{1}{2},j} = \begin{bmatrix} \rho V \\ \rho wV + n_z p \\ \rho uV + n_x p \\ \rho vV + n_y p \end{bmatrix}_{i+\frac{1}{2},j}$$

$$V = \bar{n}_{i+\frac{1}{2},j} \cdot (u,v,w)_{i+\frac{1}{2},j} \qquad (1b)$$

Equations (1) are closed using the constant total enthalpy condition and the perfect-gas equation of state that yield the constraint

$$\frac{p}{\rho}\frac{\gamma}{(\gamma-1)} + \frac{1}{2}(u^2+v^2+w^2) = H_0 \qquad (2)$$

The ZEUS code integrates Euler's equations using a second-order Godunov method. The original Godunov's method of Ref. 12 (which is applied in Ref. 11) in first-order accurate and usually cast in a control volume form. Properties within each cell are assumed constant and fluxes [$\bar{F}$ in Eqs. (1)] at cell edges are calculated using the Riemann problem. The two sets of properties adjacent to each cell edge define the two streams making up the Riemann problem. Fluxes crossing a cell edge are computed from the solution to the Riemann problem. Along any ray originating from the point of the initial stream intersection, properties are constant. The properties along the ray parallel to the cell edge are used to compute the flux. When this direction falls between the shocks/expansions defining the Riemann problem (see Fig. 4), the computed flux is influenced by properties at both adjacent cell edges. Otherwise, the cell edge flux will be a function of only one cell's properties since the flow normal to the cell edge is supersonic. The active cell is upstream or upwind of the cell edge, thus reflecting the correct domain of dependence of the problem.

Godunov's method is extended to second-order accuracy by adding a predictor step to determine properties at $z^n + \Delta z/2$ and linearly extrapolating these properties to the cell edge. The property slopes for both the predictor step and the linear extrapolation are computed using limited differences that prevent oscillations near shocks. These differences are calculated in the following manner:

$$\frac{\partial f}{\partial \xi} = \begin{cases} 0 \text{ if } (f_{i+1,j} - f_{i,j})(f_{i,j} - f_{i-1,j}) < 0 \\ \text{otherwise} \\ \dfrac{F'}{\Delta\xi}\,\text{Min}\left[\dfrac{|f_{i+1,j} - f_{i-1,j}|}{2}, \kappa'|f_{i+1,j} - f_{i,j}|, \kappa'|f_{i,j} - f_{i-1,j}|\right] \end{cases} \qquad (3)$$

where $F' = \text{sign}\,(f_{i+1,j} - f_{i,j})$ Here, f is some dependent variable differentiated with respect to some independent variable ξ.

The predictor step advances primitive variables using Euler's equations in nonconservation form. Near shocks and other discontinuities, the limiter reduces all slopes to zero and the scheme collapses to the first-order Godunov method.

Boundary Conditions

ZEUS is based on a finite-volume approach. Therefore, grid points do not lie on the boundary, but rather the cells adjacent to the wall have an edge lying along the boundary. Properties along cell edges adjacent to the wall are computed by extrapolating predicted properties to the wall using the cell slope normal to the wall. These edge properties do not satisfy the tangent flow boundary conditions and must be turned using either an oblique shock or Prandtl-Meyer expansion to satisfy the wall boundary conditions. The flow is tangent to the wall, and only the post-turn pressure influences the flux at the edge lying on the wall.

Lifting surfaces may form and disappear as the solution is marched down the length of the missile. Cell edges partially covered by a surface are divided into two elements, one containing the edge area adjacent to the surface and the other containing the edge area adjoining another cell. Separate estimates of the fluxes acting on each element are added to determine the total edge flux.

The outer zone boundary is determined by tracking the domain of dependence of the numerical solution using information contained in the Riemann problem.

Special Procedures

Artificial viscosity and other special procedures are not required by the ZEUS code. However, free parameters do occur in the difference limiters. In the program, κ' of Eq. (3) is set to 0 at cells next to fin surfaces, 1 at interior cells, and 2 at boundary cells in smooth flow regions. These values of κ' do not require adjustment from one problem to the next.

Results

The ZEUS program has been applied to several noncircular missile shapes having elliptic cross sections. These shapes included bodies-alone and a body-wing-tail. Computations were performed on the CYBER 170/865 and the SUN workstation. In all cases, the program's "self starter" initialized properties to freestream conditions at a plane a short distance from the nosetip. The marching step size ranged from 20-90% of the

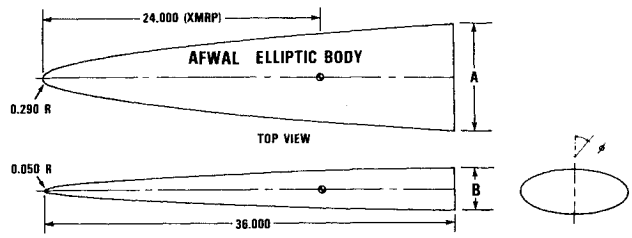

BODY	A	B
2:1	8.323	4.162
2.5:1	9.307	3.723
3:1	10.195	3.398

Fig. 6 The three AFWAL power law bodies with cross sections having ellipticity ratios of 2:1, 2.5:1, and 3:1 found in Refs. 17 and 18.

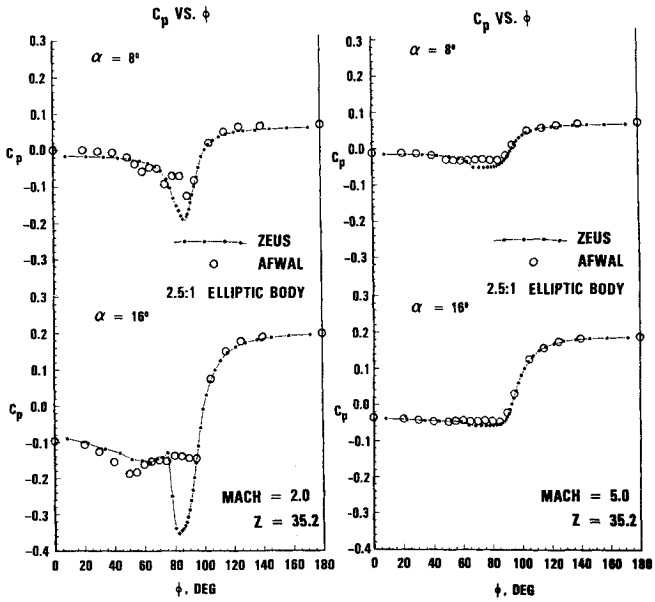

Fig. 7 Calculated and measured C_p on the AFWAL 2.5:1 elliptic body of Fig. 6 for $M_\infty = 2$ and 5, $\alpha = 8$ and 16 deg, and $z = 35.2$.

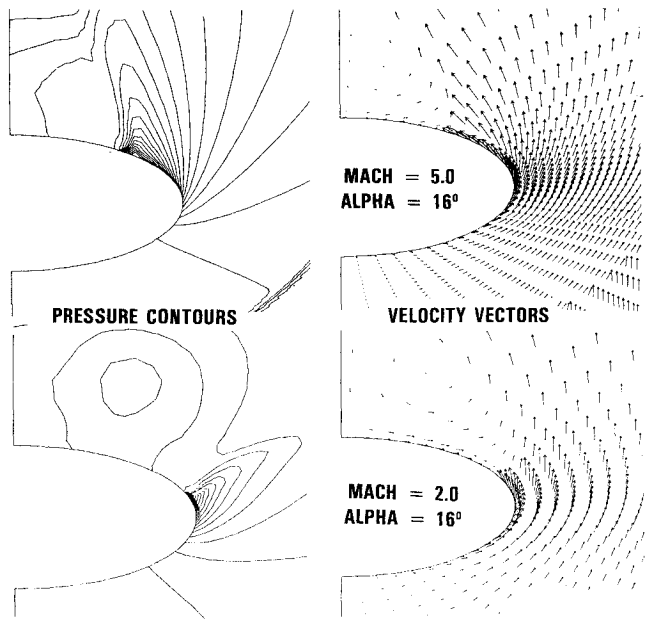

Fig. 8 Computed pressure contours and crossflow velocity vectors for the AFWAL 2.5:1 elliptic body of Fig. 6 for $M_\infty = 2$ and 5, $\alpha = 16$ deg, and $z = 35.2$.

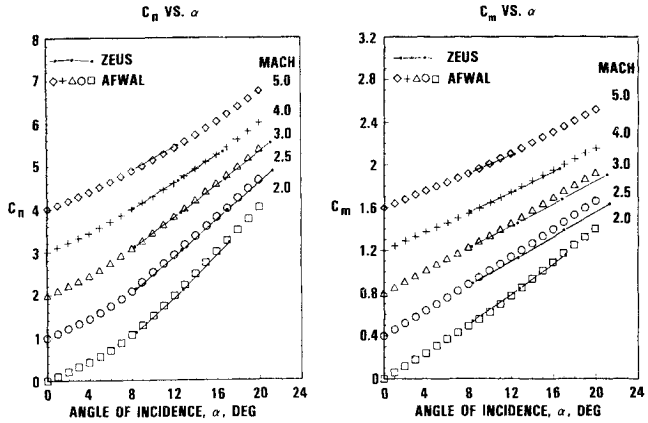

Fig. 9 Calculated and measured C_N vs α and C_M vs α for the AFWAL 3:1 elliptic body of Fig. 6 at $M_\infty = 2$–5. Each curve has its zero reference shifted by 1 for C_N vs α and 0.4 for C_M vs α.

CFL limit. Mesh points were clustered in the vicinity of the body shoulder. Computations featuring wings or tails were run using multiple zones.

Computations were performed on three Air Force Wright Aeronautical Laboratory (AFWAL) power law bodies with cross-sectional ellipticity ratios of 2:1, 2.5:1, and 3:1. These bodies were described in Refs. 17 and 18 and illustrated in Fig. 6. All of the calculations were completed using a one-zone model. Results were obtained on both a (36 × 36) and a (72 × 72) mesh. Solutions were computed for an incidence range of 0–20 deg and for the Mach numbers of 2, 2.5, 3, 4, and 5. The most noticeable feature in the computed flowfields was a crossflow shock, followed by a leeside vortex. In contrast, experiments on the same shapes exhibit a leeside vortex generated by boundary-layer separation.

Calculated and measured surface pressure coefficients for the 2.5:1 elliptic body are compared in Fig. 7, and computed pressure contours and crossflow velocities are illustrated in Fig. 8. For all the shapes, computed pressures agree well with experiment on the windward and leeward surfaces, with some discrepancies near the body shoulder where the crossflow shock occurs. In this vicinity, the solution features a crossflow shock while boundary-layer separation occurs experimentally. Although not shown here, the computed crossflow shock moves in the windward direction along the body surface with increasing body ellipticity. At least qualitatively, the primary vortex is predicted. But the secondary vortex, visible experimentally, is completely missed. At higher Mach numbers, the pressure discrepancy at the shoulder is almost negligible, as illustrated in Fig. 7. Also, the computed crossflow shock steepens, bends, and moves leeward as displayed in Fig. 8.

Normal force and pitching moment predictions on the AFWAL bodies agree well with experiment as illustrated in Fig. 9. This close agreement between calculation and experiment is a reflection of the accuracy of the computed windward and leeward pressures. Errors in the predicted pressures near the model shoulder have little influence on these quantities.

Computations have been performed on the NASA monoplane-wing missile configuration with a cross-sectional ellipticity ratio of 3:1. This shape is described in Refs. 19 and 20 and illustrated in Fig. 10. Computed results were obtained at the Mach number 2.5 over an incidence range of 0–20 deg, with and without the lifting surfaces, and at roll positions of 0 and 45 deg. At 0 deg roll, computations were completed for half of the flowfield using a one-zone model on the forebody with an (18 × 18) mesh, and a four-zone model over the wing and tails with a (36 × 36) mesh. In the case of 45 deg roll, the complete configuration was computed using a one-zone model with a (18 × 36) mesh on the forebody, and an eight-zone model with a (36 × 72) mesh over the wing and tails.

Computed flowfields on the body-alone are similar to those of the AFWAL elliptic bodies. A crossflow shock occurs

followed by a vortex. Likewise, experiments exhibit a leeside vortex; however, this vortex is generated by boundary-layer separation. The addition of the wing and tails disrupts the computed crossflow shock but does not affect the location of the vortex (see Fig. 13).

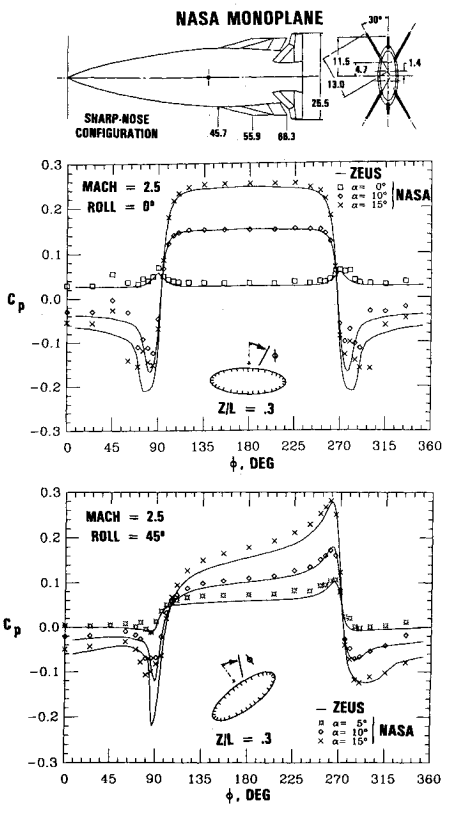

Fig. 10 Calculated and measured C_p on the NASA monoplane-wing missile of Refs. 19 and 20 for $M_\infty = 2.5$, $\alpha = 0$–15 deg, roll orientations = 0 and 45 deg, and $z/L = 0.3$.

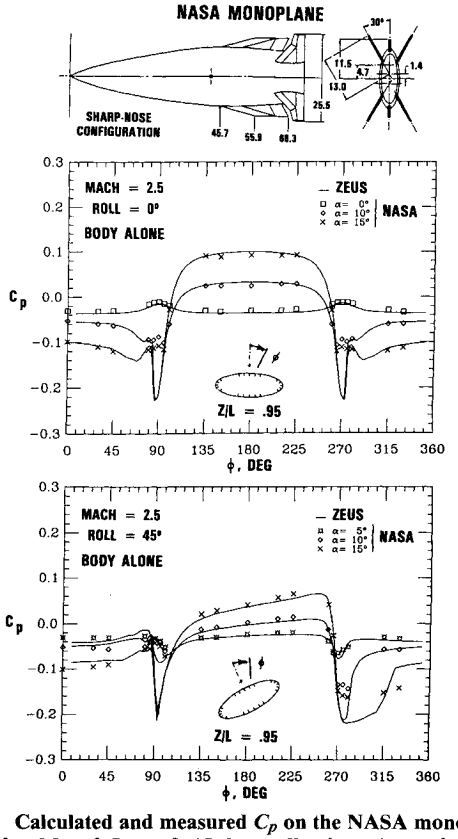

Fig. 11 Calculated and measured C_p on the NASA monoplane-wing missile for $M_\infty = 2.5$, $\alpha = 0$–15 deg, roll orientations = 0 and 45 deg, and $z/L = 0.95$ for the body-alone.

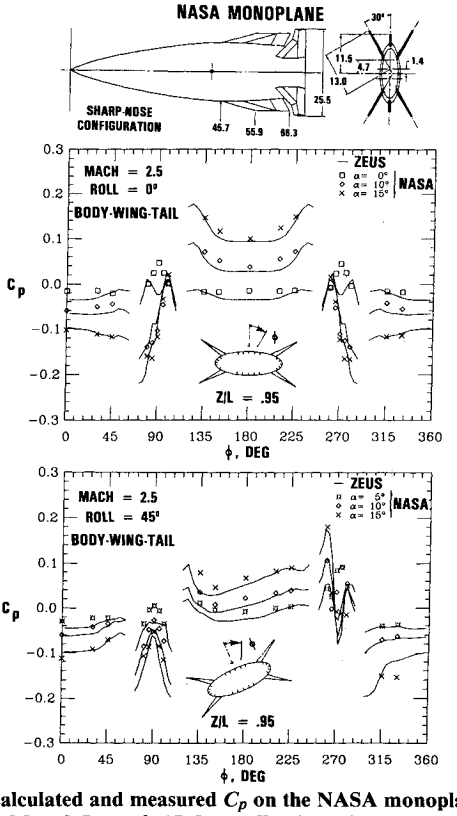

Fig. 12 Calculated and measured C_p on the NASA monoplane-wing missile for $M_\infty = 2.5$, $\alpha = 0$–15 deg, roll orientations = 0 and 45 deg, and $z/L = 0.95$ for the body-wing-tail.

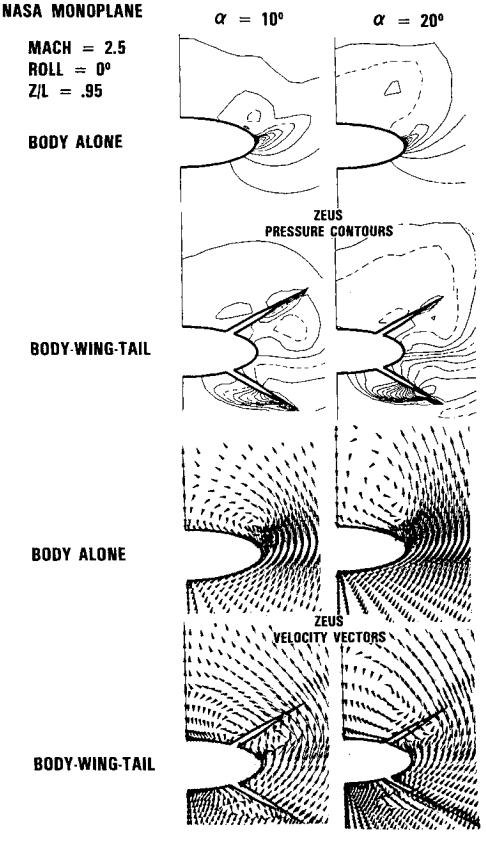

Fig. 13 Computed pressure contours and crossflow velocity vectors for the NASA monoplane of Fig. 10 for $M_\infty = 2.5$, $\alpha = 10$ and 20 deg, roll orientation = 0 deg, and $z/L = 0.95$ for the body-alone and the body-wing-tail.

Calculated and measured surface pressures are compared in Figs. 10–12 for the 0 and 45 deg roll orientations. Crossflow plane pressure contours and velocities are illustrated in Figs. 13 and 14 for 0 and 45 deg roll, respectively. Close agreement between calculated and measured pressures is achieved on the windward and leeward surfaces, with discrepancies at the body shoulder. These discrepancies diminish with the addition of the lifting surfaces, and predicted results agree well with experiment, as illustrated in Figs. 10–12. Increases in incidence have little effect on the accuracy of the computed surface pressures, but they do affect the strength of the crossflow shock. The vortex behind the computed crossflow shock on the body-alone lifts further off the surface with increasing angle of attack, as illustrated in Figs. 13 and 14. Addition of the tails disrupts the crossflow shock but does not change the location of the vortex.

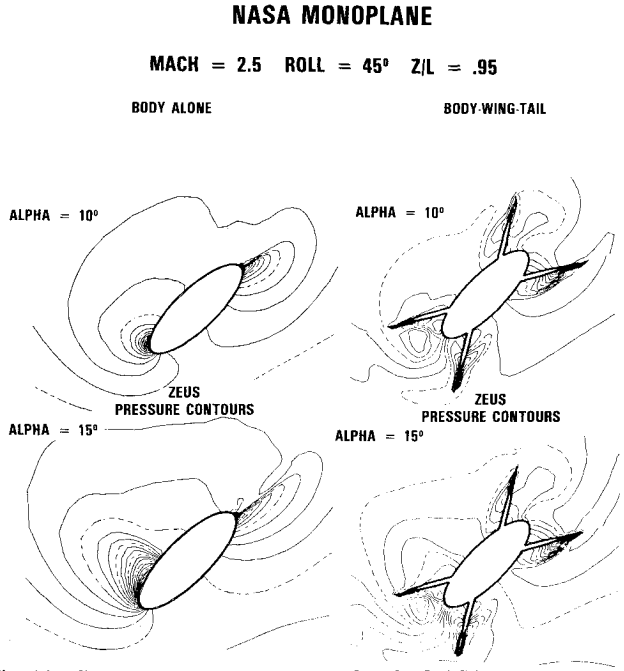

Fig. 14 Computed pressure contours for the NASA monoplane of Fig. 10 for $M_\infty = 2.5$, $\alpha = 10$ and 15 deg, roll orientation = 45 deg, and $z/L = 0.95$ for the body-alone and the body-wing-tail.

Normal force and pitching moment variations with angle of attack are shown in Fig. 15 for the NASA body-alone and body-wing-tail shapes at 0 deg roll. Computations show good agreement with experiment as a result of the well-predicted pressures on both sides of the body. Increments in normal force due to the presence of the wing and tails also agrees well with experiment over the full incidence range. But moments (referenced at $0.6L$ from the nose) are slightly displaced when the lifting surfaces are added.

Concluding Remarks

This paper has investigated the application of the ZEUS code to missile shapes having elliptic cross sections. Computed surface pressure distributions agree well with experiment on the windward and leeward surfaces, with some discrepancies at the body shoulder. Near this region, computations produce a crossflow shock followed by a vortex, while experiment generates a vortex through boundary-layer separation. The change in body shape and Mach number affects the location and shape of the computed crossflow shock. Computed surface pressure discrepancies at the shoulder are shown to have little effect on the accurate prediction of the aerodynamic coefficients. Finally, for elliptic bodies with lifting surfaces, ZEUS computed both well-predicted surface pressures and overall aerodynamics.

Acknowledgments

This work was supported by the Naval Surface Warfare Center Independent Research and the Naval Air Systems Command. The project monitor was Dale Hutchins (AIR-310-C).

References

[1]Hoeijmakers, H. W. M. "The Role of Computational Fluid Dynamics in Missile Aerodynamics," Missile Aerodynamics Conference, Nielsen Engineering and Research, Inc., Monterey, CA, Oct. 1988.

[2]Moretti, G., Grossman, B., and Marconi, F., "A Complete Numerical Technique for the Calculation of Three-Dimensional Inviscid Supersonic Flow," AIAA Paper 72-192, 1972.

[3]Kutler, P., Reinhardt, W. A., and Warming, R. F., "Multishocked, Three-Dimensional Supersonic Flowfields with Real Gas Effects," *AIAA Journal,* Vol. 11, May 1973, pp. 657–664.

[4]Moretti, G., "Conformal Mappings for Computation of Steady, Three-Dimensional, Supersonic Flows," *Numerical/Laboratory Computer Methods in Fluid Dynamics,* Vol. 13, 1976.

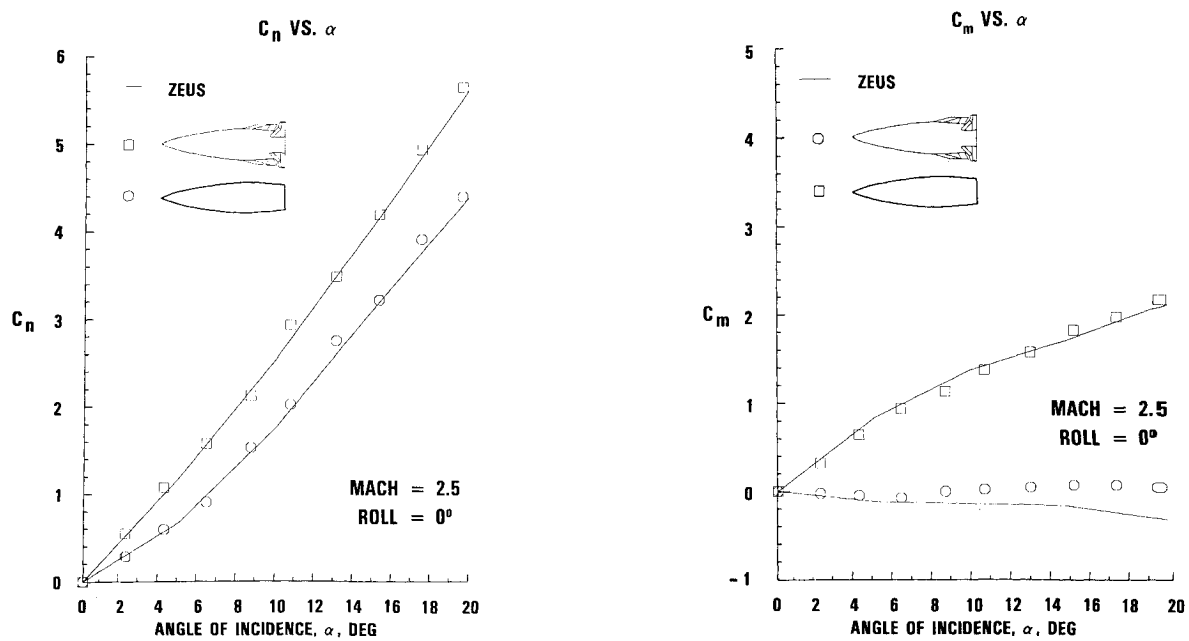

Fig. 15 Calculated and measured C_N vs α and C_M vs α on the NASA monoplane-wing missile at 0 deg roll orientation for the body-alone and the body-wing-tail.

[5]Solomon, J. M., Ciment, M., Ferguson, R. E., and Bell, J. B., "Inviscid Flowfield Calculations for Reentry Vehicles with Control Surfaces," *AIAA Journal,* Vol. 15, Dec. 1977, pp. 1742–1749.

[6]Wardlaw, A. B., Jr., Solomon, J. M., and Baltakis, F. P., "Supersonic Inviscid Flowfield Computations for Missile Type Bodies," *AIAA Journal,* Vol. 19, July 1981, pp. 899–906.

[7]Wardlaw, A. B., Jr., Baltakis, F. P., Solomon, J. M., and Hackerman, L. B., "An Inviscid Computational Method for Tactical Missile Configurations," Naval Surface Warfare Center, Silver Spring, MD, NSWC TR 81-457, Dec. 1981.

[8]Wardlaw, A. B., Jr., Priolo, F. J., Solomon, J. M., and Baltakis, F. P., "Inviscid Multiple Zone Calculations for Supersonic Tactical Missiles," AIAA Paper 84-2099, Aug. 1984.

[9]Priolo, F. J., Wardlaw, A. B., Jr., Baltakis, F. P., and Solomon, J. M., "Inviscid Multiple Zone Strategy Applied to Complicated Supersonic Tactical Missile Configurations," AIAA Paper 85-1813, Aug. 1985.

[10]Wardlaw, A. B., Jr., Priolo, F. J., and Solomon, J. M., "A Multiple Zone Method for Supersonic Tactical Missiles," Naval Surface Warfare Center, Silver Spring, MD, NSWC TR 85-484, June 1986.

[11]Wardlaw, A. B., Jr., Baltakis, F. P., Martin, F. M., Priolo F. J., and Jettmar, R. U., "Godunov's Method for Supersonic Tactical Missile Computations," *Journal of Spacecraft and Rockets,* Vol. 24, Jan.-Feb. 1987, pp. 40–47.

[12]Godunov, S. K., "A Difference Method for the Numerical of Discontinuous Solutions of the Equations of Calculation/Hydrodynamics," *Mathematics Zbornik,* 47, 1959, pp. 271–290 (in Russian).

[13]Wardlaw, A. B., Jr. and Davis, S. F., "A Second Order Godunov Method for Tactical Missiles," AGARD, CP-412, Nov. 1986, pp. 12.1–12.10.

[14]Wardlaw, A. B., Jr. and Davis, S. F., "A Second Order Godunov Method for Supersonic Tactical Missiles," Naval Surface Warfare Center, Silver Spring, MD, NSWC TR 86-506, Dec. 1986.

[15]Wardlaw, A. B., Jr. and Priolo, F. J., "Applying the ZEUS Code," Naval Surface Warfare Center, Silver Spring, MD, NSWC TR 86-508, Dec. 1986.

[16]Davis, S. F., "Simplified Second Order Godunov-Type Methods," *SIAM Journal on Scientific and Statistical Computing,* Vol. 9, May 1988, pp. 445–473.

[17]Shereda, D. E., Amidon, P. F., Dahlem, V., III, and Brown-Edwards, E., "Pressure Test of Three Elliptical Missile Body Configurations at Mach Numbers 1.5 to 5.0," Wright-Patterson AFB, OH, AFWAL TM 84-236-FIMG, Dec. 1984.

[18]Amidon, P. F. and Dahlem, V., III, "Flow Visualization Test of Three Elliptical Missile Body Configurations at Mach Numbers 1.5 to 5.0," Wright Patterson AFB, OH, AFWAL TM 86-188-FIMG, May 1986.

[19]Allen, J. M., Hernandez, G., and Lamb, M., "Body-Surface Pressure Data on Two Monoplane-Wing Missile Configurations With Elliptical Cross Sections at Mach 2.50," NASA TM-85645, Sept. 1983.

[20]Graves, E. B. and Fournier, R. H., "Effect of Nose Bluntness and Afterbody Shape on Aerodynamic Characteristics of a Monoplanar Missile Concept With Bodies of Circular and Elliptical Cross Sections at a Mach Number of 2.50," NASA TM-80055, 1979.